

Millimetre observations of infrared carbon stars

II. Mass loss rates and expansion velocities

M. A. T. Groenewegen¹, M. Sevenster², H. W. W. Spoon³, and I. Pérez^{2,4}

¹ Instituut voor Sterrenkunde, PACS-ICC, Celestijnenlaan 200B, 3001 Heverlee, Belgium

² Mount Stromlo and Siding Spring Observatory, Cotter road, Weston ACT, Australia

³ Kapteyn Astronomical Institute, Postbus 800, 9700 AV, Groningen, The Netherlands

⁴ Departamento de Astronomía, Universidad de Chile, Casilla 36-D, Santiago, Chile

Received 1 March 2002 / Accepted 15 May 2002

Abstract. Dust- and gas mass loss rates and distances are determined for a sample of about 330 infra-red carbon stars that probe a distance up to about 5.5 kpc. The dependence of the dust- and gas mass loss rates, and the expansion velocity upon galactic longitude (l) are studied. It is found that the expansion velocity significantly depends on l , but that the absolute bolometric magnitude, the dust mass loss rate and the gas-to-dust ratio depend on l marginally, if at all, and the gas mass loss rate does not depend on l . Beyond the solar circle, the expansion velocity (as well as the luminosity, dust-to-gas ratio, dust mass loss rate) is lower than inside the solar circle, as expected from the overall gradient in metallicity content of the Galaxy. Combining the average expansion velocity inside and beyond the solar circle with the theoretically predicted relation between expansion velocity and gas-to-dust ratio, we find that the metallicity gradient in the solar neighbourhood is about -0.034 dex/kpc, well within the quoted range of values in the literature.

Key words. circumstellar matter – stars: mass loss – stars: AGB and post-AGB – radio lines: stars

1. Introduction

In the accompanying paper (Groenewegen et al. 2002, hereafter G2002) a sample of 380 infra-red carbon stars is selected based on IRAS 12 and 25 μm fluxes. The main aim of the project is to analyse the radial velocities for these stars in order to study their dynamical properties and compare the outcome to previous results on optical carbon stars and on OH/IR stars (Sevenster et al. 1995, 2000). The most efficient way to obtain the radial velocities for infra-red carbon stars is by the millimetre emission of molecules in their extended circumstellar shells.

About 120 stars in the sample selected in G2002 have published radial velocities, and the focus in G2002 has been on the millimetre observations of the remaining about 250 objects, resulting in about 200 detections.

Besides the radial velocity, the millimetre observations yield the expansion velocity of the circumstellar shell and the peak intensity and integrated line intensity of the lines observed. These are more traditional observational quantities that are used to determine mass loss rates (e.g. Schöier & Olofsson 2001; Groenewegen & de Jong 1998; Kerschbaum & Olofsson 1998).

In the present paper, the new data on 200 infra-red carbon stars are combined with data of 120 objects in the literature in order to derive the dust- and gas mass loss rates and investigate the spatial dependence of mass loss and expansion velocity.

The sample is introduced in Sect. 2, and the analysis is carried out in Sect. 3. The analyses in terms of distribution functions and the comparison to the dynamical properties of other populations of evolved stars will be reported elsewhere (Sevenster et al. 2002, in preparation).

2. The sample

The selection of the sample of infra-red carbon stars is explained in G2002. In brief, objects fulfill the following criteria: IRAS PSC Flux quality 3 at 12 and 25 μm , and ≥ 2 at 60 μm , flux ratios $S_{12}/S_{25} < 3$, $S_{25}/S_{60} > 2.75$, and finally $S_{12} > 20$ Jy or IRAS LRS classification equal to 4n. Stars associated with non-carbon star spectral types were excluded, and the LRS spectra were visually inspected to look for the silicate feature in order to exclude these stars as well. In addition, the SIMBAD database was checked for references to SiO or OH thermal or maser line observations. About ten extremely red carbon stars were added that fulfilled the flux criteria mentioned above.

The total sample contains 380 stars. Of those 124 stars had a reliable radial velocity reported (from the Loup et al. 1993 catalog, Kastner et al. 1993 and Groenewegen et al. 1996).

Send offprint requests to: M. Groenewegen,
e-mail: groen@ster.kuleuven.ac.be

Recent papers that were also consulted are Neri et al. 1998; Knapp et al. 1998; Josselin et al. 1998 for improved observations for a few of these stars). The others were put on the observing list and G2002 report on the millimetre observations of the remaining about 260 stars, of which about 200 were detected.

Table 1 lists the stars used in the analysis (first the data on the 207 new observations in order of RA, followed by the data on the 124 stars from the literature in order of RA). Listed are the IRAS name and Galactic longitude and latitude; the expansion velocity and radial velocity w.r.t. the LSR are taken from G2002 and the literature cited above, taking a mean value when multiple observations exist. The remaining columns give the apparent and absolute bolometric magnitude, the distance, gas- and dust mass loss rate and the gas-to-dust ratio. These quantities have been derived, as explained in the next section. Additional input for the calculations discussed below are the IRAS 60 μm flux and the CO line peak intensity. The latter are not explicitly repeated here and are taken from G2002 and the literature cited above. The CO (2–1) line is preferred over the CO (1–0) line when both have been measured.

3. Analysis

3.1. Bolometric magnitudes

There are several possible ways to calculate the apparent bolometric magnitude but only the IRAS 12 and 25 μm fluxes are available for *all* stars. Therefore, the apparent bolometric magnitudes are calculated from

$$m_{\text{bol}} = m_{12} + \text{BC}_{12} \quad (1)$$

with the bolometric correction at 12 μm for carbon stars taken from Loup et al. (2002).

Out of the 331 objects, 68 have a known pulsation period (from the GCVS [Kholopov et al. 1985]; Jones et al. 1990; Le Bertre 1992; Joyce et al. (private communication 1997), Whitelock et al. 2000; Nakashima et al. 2000; Olivier et al. 2001), with periods in the range 233 to 1060 days, and for these the absolute bolometric magnitude is calculated from the $(M_{\text{bol}} - P)$ -relation in Groenewegen & Whitelock (1996). Their relation was derived in the period range 150–520 days but is assumed to hold for longer periods as well. For these infra-red objects one would also expect a relation between luminosity and the ratio (S_{25}/S_{12}) , as stars with higher luminosities tend to have higher mass loss rates, which implies redder colours. Figure 1 plots the M_{bol} obtained from the $(M_{\text{bol}} - P)$ -relation versus $\log(S_{25}/S_{12})$. There is indeed an obvious correlation. A linear fit to the 64 stars with $P > 390$ days gives:

$$M_{\text{bol}} = -0.93 (\pm 0.16) \log(S_{25}/S_{12}) - 5.40 (\pm 0.05) \quad (2)$$

with a dispersion of 0.17 mag. This dispersion is smaller than the dispersion of 0.26 in the $(M_{\text{bol}} - P)$ -relation in Groenewegen & Whitelock (1996), indicating the usefulness of this relation in the regime of long-period variables. There are 4 objects with periods less than 390 days, namely 20084-1425 (345 d; the mira variable R Cap), 21197-6956 (233 d; the SRb variable Y Pav), 05426+2040 (242 d; the SRa variable Y Tau) and

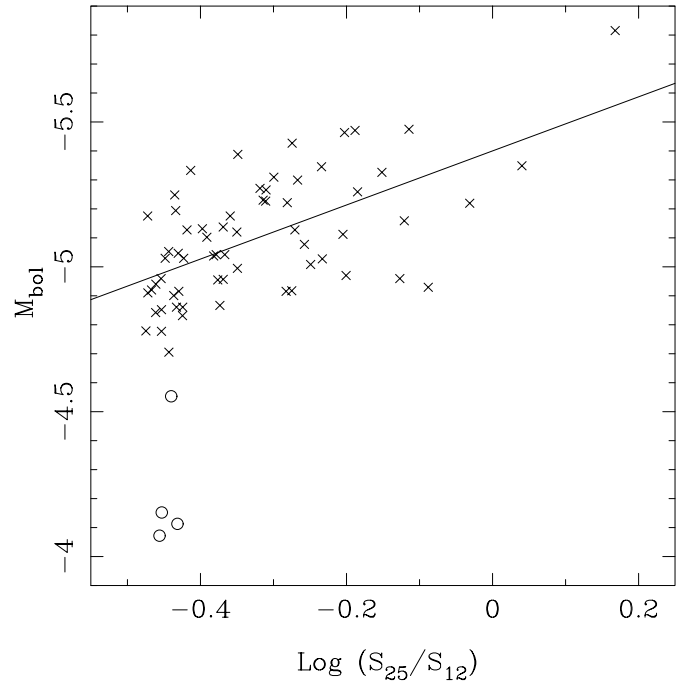


Fig. 1. M_{bol} versus $\log(S_{25}/S_{12})$ flux-ratio. A linear fit is indicated (see text), where the points represented by the open circles have been excluded.

17389-5742 (225 d; the SRa variable V Pav). They all have $\log(S_{25}/S_{12}) < -0.4$ and $M_{\text{bol}} > -4.7$. Of all the SR variables in the sample, these three have the shortest period and likely the *PL*-relation derived originally for mira variables does not apply.

3.2. Distances

Distances are calculated from the apparent bolometric magnitude and the absolute bolometric magnitude, which is based on the $(M_{\text{bol}} - P)$ -relation in Groenewegen & Whitelock (1996) for the stars with a pulsation period longer than 390 days, and based on Eq. (2) for all other objects, neglecting reddening. Values for the distance, absolute and apparent magnitude are listed in Table 1. Realistic 1σ errors are probably ± 0.2 in the magnitudes and 15% in distance.

Figure 2 shows the projection of the stars onto the galactic plane (with circles of radius 1 and 2 kpc around the Sun indicated) and the plane $X = 0$. A distinction is made between northern and southern sources in this plot to see if the mixing of observations of different telescopes (mainly SEST and IRAM) might have introduced any detection bias, but from the uniform distribution onto the Galactic plane this appears not to be the case, and in the analysis below the sample is therefore treated uniformly.

The average of the absolute value of the distance to the Galactic plane is 295 pc. Since the limiting distance is much larger than this, the typical scale height is also close to 295 pc. This is in good agreement with values between 200 and 300 pc quoted in the literature (Claussen et al. 1987; Jura & Kleinmann 1989; Groenewegen et al. 1992).

Table 1. Data on the stars used in this study.

IRAS Name	l	b	v_e (km s ⁻¹)	v_{LSR} (km s ⁻¹)	m_{bol} (mag)	M_{bol} (mag)	d (kpc)	\dot{M}_g (M_{\odot} yr ⁻¹)	\dot{M}_d (M_{\odot} yr ⁻¹)	\dot{M}_g/\dot{M}_d
00422+5310	122.0	-9.4	13.6	19.4	8.08	-5.00	4.11	0.361E-05	0.980E-08	368.
01080+5327	125.9	-9.0	22.6	-20.0	6.39	-5.03	1.92	0.640E-05	0.107E-07	596.
01443+6417	129.0	2.3	30.5	-68.1	6.96	-5.03	2.49	0.175E-04	0.180E-07	971.
02345+5422	138.1	-5.1	19.8	-66.0	7.96	-5.42	4.74	0.775E-04	0.942E-07	822.
02596+6639	135.4	7.3	15.8	-41.8	8.42	-5.02	4.88	0.643E-05	0.111E-07	578.
03157+3258	155.3	-20.3	15.2	-16.6	7.60	-5.17	3.58	0.858E-05	0.239E-07	359.
03238+6034	140.9	3.5	15.3	-85.5	7.12	-4.92	2.55	0.116E-04	0.208E-07	558.
03277+5120	146.6	-3.9	17.1	-29.5	8.45	-5.02	4.93	0.563E-05	0.125E-07	452.
03293+6038	141.4	3.9	21.0	-61.9	7.60	-5.19	3.61	0.349E-04	0.339E-07	1030.
03385+5927	143.1	3.6	16.5	-74.7	7.33	-5.20	3.21	0.645E-05	0.261E-07	247.
03557+4402	154.8	-6.8	14.9	-48.4	7.88	-4.93	3.64	0.760E-05	0.433E-07	175.
04127+5030	152.6	0.0	17.5	0.3	7.33	-4.91	2.80	0.399E-05	0.927E-08	430.
04179+5951	146.6	7.2	21.8	5.2	7.26	-5.09	2.95	0.194E-04	0.292E-07	666.
04297+2941	169.9	-12.3	17.5	4.4	7.69	-5.13	3.65	0.772E-05	0.282E-07	273.
04365+6349	145.1	11.5	14.2	-47.0	8.11	-5.07	4.32	0.117E-04	0.166E-07	702.
04369+4504	159.3	-0.9	20.9	24.1	8.37	-5.09	4.92	0.146E-04	0.243E-07	602.
04449+4951	156.6	3.3	40.0	-3.7	6.61	-4.96	2.07	0.886E-05	0.123E-07	719.
05223+4705	162.6	6.5	37.4	-11.0	6.94	-5.04	2.48	0.112E-04	0.284E-07	395.
05261+4626	163.5	6.7	12.5	-58.1	8.27	-5.08	4.67	0.755E-05	0.151E-07	500.
05316+1757	188.0	-7.9	15.8	35.4	7.71	-4.99	3.47	0.415E-05	0.971E-08	427.
05428+1215	194.3	-8.6	16.4	23.0	8.17	-4.92	4.15	0.464E-05	0.107E-07	434.
05440+4311	167.9	7.7	20.0	-45.7	7.57	-5.01	3.27	0.525E-05	0.240E-07	219.
05447+1321	193.6	-7.6	21.5	6.3	8.43	-5.15	5.20	0.254E-04	0.375E-07	677.
06088+1902	191.5	0.3	x	62.0	7.09	-5.06	2.68	x	x	x
06181+0402	205.8	-4.9	18.3	31.3	7.91	-5.36	4.51	0.299E-04	0.578E-07	518.
06183+1135	199.2	-1.4	18.6	-3.2	6.35	-4.97	1.84	0.125E-05	0.873E-08	143.
06192+0722	203.0	-3.2	24.2	15.2	7.10	-5.18	2.86	0.110E-04	0.144E-07	766.
06315+1602	196.7	3.6	14.9	24.9	7.48	-5.04	3.20	0.471E-05	0.153E-07	309.
06323+3015	184.1	10.1	15.8	6.6	7.87	-5.08	3.89	0.131E-04	0.166E-07	785.
06344-0124	212.6	-3.9	17.7	59.6	8.15	-5.36	5.05	0.104E-04	0.750E-07	138.
06348+3114	183.4	11.0	22.0	29.6	8.31	-5.12	4.86	0.165E-04	0.332E-07	496.
06378-0527	216.6	-5.0	20.6	42.2	8.01	-5.14	4.25	0.288E-04	0.369E-07	778.
06447+0817	205.1	2.9	24.4	68.4	8.41	-4.92	4.62	0.147E-04	0.327E-07	449.
06462-4157	251.4	-18.4	7.6	-17.6	8.11	-5.17	4.53	0.273E-05	0.139E-07	197.
06471+0305	210.1	1.0	19.9	51.1	7.60	-5.08	3.42	0.702E-05	0.235E-07	299.
06528-4218	252.2	-17.4	12.0	15.1	7.07	-4.98	2.57	0.329E-05	0.950E-08	346.
06585-4111	251.5	-16.0	27.9	50.0	7.42	-4.99	3.04	0.155E-04	0.149E-07	1038.
07073-1944	232.6	-5.1	19.4	54.6	8.43	-5.20	5.31	0.335E-04	0.385E-07	870.
07080-0104	216.2	3.7	25.4	38.6	7.67	-5.12	3.63	0.920E-05	0.369E-07	250.
07085-0018	215.5	4.2	20.3	62.7	7.81	-5.13	3.87	0.338E-04	0.329E-07	1027.
07149-0046	216.7	5.4	17.0	54.7	8.25	-5.16	4.83	0.328E-04	0.360E-07	910.
07161-0111	217.2	5.5	43.0	20.6	7.29	-5.04	2.92	0.808E-05	0.416E-07	194.
07170+0721	209.6	9.6	17.6	65.5	7.86	-5.12	3.94	0.520E-05	0.246E-07	212.
07220-2324	237.5	-3.8	x	30.0	7.53	-5.12	3.38	x	x	x
07266-0541	222.4	5.7	14.1	76.9	7.68	-5.33	3.99	0.917E-05	0.400E-07	229.
07336-1004	227.1	5.1	34.0	45.5	7.49	-5.13	3.35	0.449E-04	0.515E-07	871.
07356-3549	249.8	-7.1	13.7	-14.1	8.44	-5.03	4.94	0.765E-05	0.116E-07	660.
07368-2833	243.6	-3.4	19.7	62.8	7.78	-5.16	3.86	0.250E-04	0.286E-07	874.
07373-4021	254.0	-9.0	21.4	19.6	5.45	-5.00	1.23	0.697E-05	0.987E-08	706.
07546-2551	243.3	1.4	20.2	96.5	8.89	-5.09	6.26	0.161E-04	0.257E-07	627.
08086-3905	256.0	-3.2	17.0	24.3	7.92	-5.32	4.44	0.197E-04	0.518E-07	381.
08119-3627	254.2	-1.2	19.0	-5.3	7.26	-5.00	2.83	0.837E-05	0.721E-08	1160.
08129-1236	234.3	12.1	16.7	39.5	7.96	-5.10	4.08	0.775E-05	0.206E-07	376.
08250-2603	247.2	7.0	17.3	60.0	7.36	-4.99	2.95	0.652E-05	0.984E-08	663.
08276-5125	268.1	-7.4	20.3	31.5	8.46	-5.35	5.78	0.515E-04	0.657E-07	783.
08305-3314	253.8	3.8	28.7	58.3	7.75	-5.38	4.21	0.135E-03	0.106E-06	1272.
08340-3357	254.8	3.9	22.5	48.1	6.33	-5.07	1.91	0.911E-05	0.215E-07	423.
08353-3424	255.3	3.9	22.0	24.2	7.04	-4.99	2.54	0.477E-05	0.110E-07	436.

Table 1. continued.

IRAS Name	l	b	v_e (km s ⁻¹)	v_{LSR} (km s ⁻¹)	m_{bol} (mag)	M_{bol} (mag)	d (kpc)	\dot{M}_g (M_{\odot} yr ⁻¹)	\dot{M}_d (M_{\odot} yr ⁻¹)	\dot{M}_g/\dot{M}_d
08416–2525	248.9	10.4	17.1	-18.1	6.67	-5.02	2.18	0.113E-04	0.120E-07	936.
08439–2734	251.0	9.5	15.0	71.2	7.33	-5.11	3.07	0.128E-04	0.137E-07	939.
08470–5710	274.5	-8.6	25.8	-4.8	8.08	-5.10	4.33	0.227E-04	0.364E-07	622.
08534–5055	270.2	-3.9	26.6	8.5	7.23	-5.23	3.10	0.491E-04	0.522E-07	941.
08535–4724	267.6	-1.6	17.1	43.5	7.26	-5.25	3.17	0.685E-05	0.436E-07	157.
08544–4431	265.5	0.4	8.2	46.4	6.14	-5.35	1.98	0.108E-05	0.616E-07	18.
08556–5717	275.3	-7.8	17.3	-38.5	7.93	-5.06	3.96	0.108E-04	0.178E-07	611.
09176–5147	273.4	-1.7	23.7	44.1	7.50	-5.08	3.28	0.106E-04	0.322E-07	330.
09178–5556	276.4	-4.6	20.1	39.4	8.80	-5.23	6.40	0.400E-04	0.454E-07	882.
09238–5305	275.1	-2.0	12.7	45.6	8.22	-5.17	4.77	x	x	x
09317–5116	274.7	0.2	11.4	13.9	7.83	-5.37	4.37	0.229E-04	0.398E-07	575.
09428–4341	271.1	7.1	18.4	17.8	7.74	-5.03	3.58	0.802E-05	0.149E-07	536.
09450–4716	273.7	4.6	x	5.9	7.79	-5.35	4.24	x	x	x
09485–4232	271.1	8.6	14.2	-4.2	8.14	-5.09	4.43	0.640E-05	0.170E-07	376.
09496–5050	276.5	2.3	25.4	37.6	8.06	-5.26	4.62	0.278E-04	0.633E-07	440.
09533–6021	282.9	-4.8	19.9	5.9	8.06	-5.21	4.51	0.220E-04	0.321E-07	687.
09587–5056	277.7	3.1	x	3.0	8.16	-5.21	4.72	x	x	x
10002–4641	275.4	6.7	x	34.7	7.72	-5.06	3.59	x	x	x
10068–6341	286.1	-6.5	37.6	-6.7	7.27	-4.96	2.79	0.111E-04	0.123E-07	907.
10098–5742	283.0	-1.4	15.2	-34.6	7.81	-5.21	4.02	0.129E-04	0.461E-07	280.
10249–2517	266.4	26.9	14.6	14.0	6.89	-4.83	2.21	0.480E-05	0.790E-08	608.
10375–4801	281.4	9.0	22.6	-6.6	7.91	-5.20	4.18	0.257E-04	0.316E-07	814.
10558–6537	291.7	-5.5	x	-37.2	7.86	-4.96	3.67	x	x	x
11073–6325	291.9	-3.0	11.8	1.2	8.49	-5.17	5.40	0.762E-05	0.174E-07	437.
11186–5528	290.4	4.9	17.2	-28.1	5.78	-5.02	1.45	0.103E-04	0.122E-07	844.
11272–6902	295.8	-7.6	26.6	-39.7	7.91	-5.09	3.97	0.129E-04	0.354E-07	363.
11463–6320	296.0	-1.6	x	3.0	7.77	-5.26	4.04	x	x	x
11514–5841	295.6	3.1	17.8	-16.8	7.61	-5.29	3.80	0.184E-04	0.421E-07	437.
12042–6355	298.1	-1.8	x	-14.1	7.59	-5.52	4.19	x	x	x
12142–6410	299.2	-1.8	34.0	-37.2	8.41	-5.19	5.25	0.643E-04	0.487E-07	1320.
12195–6830	300.3	-6.1	16.9	-62.9	7.95	-5.36	4.61	0.119E-04	0.607E-07	196.
12227–5045	298.8	11.6	15.2	23.4	8.18	-5.06	4.44	0.197E-04	0.137E-07	1436.
12298–5754	300.4	4.6	20.2	-28.9	6.37	-5.15	2.02	0.181E-04	0.340E-07	531.
12397–6447	302.0	-2.2	24.5	-24.1	8.31	-5.31	5.29	0.338E-04	0.603E-07	561.
12419–6058	302.1	1.6	15.2	-59.6	7.20	-5.44	3.36	0.317E-04	0.619E-07	511.
12550–7405	303.4	-11.5	13.1	-25.8	8.93	-5.35	7.20	0.256E-04	0.515E-07	498.
12562–6005	303.9	2.5	18.5	-36.4	7.83	-5.31	4.24	0.142E-04	0.523E-07	271.
12595–6035	304.3	2.0	16.6	-52.2	8.80	-5.27	6.53	0.406E-04	0.893E-07	455.
13031–5743	304.9	4.8	10.9	-79.6	7.62	-5.04	3.41	0.479E-05	0.109E-07	440.
13045–6404	304.7	-1.5	13.6	-70.8	7.58	-5.30	3.77	0.195E-04	0.360E-07	543.
13053–6341	304.8	-1.1	x	-23.0	7.49	-5.35	3.69	x	x	x
13343–5613	309.3	5.8	12.6	-44.9	6.90	-4.84	2.23	0.228E-05	0.679E-08	335.
13343–5801	309.0	4.0	13.0	-6.3	7.27	-5.21	3.13	0.477E-05	0.279E-07	171.
13482–6716	308.7	-5.3	18.2	-36.5	6.44	-5.06	1.99	0.137E-04	0.195E-07	701.
13509–6348	309.8	-2.0	8.3	-28.6	7.17	-5.21	3.00	0.406E-05	0.185E-07	219.
14010–5927	312.0	1.9	x	-23.5	8.14	-5.03	4.31	x	x	x
14122–5845	313.6	2.1	x	-12.5	7.25	-5.01	2.83	x	x	x
14284–5245	317.8	7.0	17.3	-71.0	8.28	-5.30	5.21	0.187E-04	0.529E-07	354.
14309–5126	318.7	8.0	14.8	-3.1	7.21	-4.98	2.74	0.276E-05	0.716E-08	385.
14358–6302	314.8	-2.9	x	-43.0	7.37	-5.24	3.32	x	x	x
14404–6320	315.1	-3.4	16.8	-76.2	7.40	-5.22	3.33	0.822E-05	0.287E-07	286.
14443–5702	318.2	2.0	26.6	-60.3	7.72	-5.33	4.09	0.272E-04	0.756E-07	360.
14521–6058	317.4	-1.9	24.8	-38.1	8.08	-5.06	4.25	0.228E-04	0.327E-07	696.
15043–5438	321.8	3.0	17.9	-15.9	6.80	-5.03	2.32	0.694E-05	0.140E-07	496.
15054–5458	321.8	2.6	21.4	-67.2	8.08	-5.53	5.25	0.619E-04	0.127E-06	486.
15471–5644	325.6	-2.2	21.7	-31.6	6.37	-5.54	2.41	0.126E-04	0.139E-06	91.
15488–4928	330.4	3.4	22.6	-63.2	6.94	-5.26	2.75	0.223E-04	0.490E-07	455.

Table 1. continued.

IRAS Name	l	b	v_e (km s ⁻¹)	v_{LSR} (km s ⁻¹)	m_{bol} (mag)	M_{bol} (mag)	d (kpc)	\dot{M}_g (M_{\odot} yr ⁻¹)	\dot{M}_d (M_{\odot} yr ⁻¹)	\dot{M}_g/\dot{M}_d
16047–5449	328.8	-2.3	x	-46.9	6.70	-4.98	2.16	x	x	x
16123–4654	335.0	2.7	11.7	-58.7	7.99	-5.17	4.28	0.941E-05	0.192E-07	491.
16171–4759	334.8	1.4	23.3	38.7	7.38	-5.11	3.14	0.217E-04	0.301E-07	719.
16296–4417	339.0	2.4	19.6	-74.1	7.98	-5.24	4.41	0.132E-04	0.505E-07	261.
16298–5349	332.1	-4.2	20.2	27.0	8.19	-5.20	4.76	0.192E-04	0.398E-07	481.
16304–3831	343.3	6.2	9.7	-15.8	8.28	-5.14	4.83	0.247E-05	0.143E-07	173.
16469–4753	338.3	-2.2	17.5	-76.9	8.06	-5.55	5.27	0.149E-04	0.121E-06	123.
16562–5039	337.1	-5.2	19.7	-58.0	7.07	-5.02	2.62	0.632E-05	0.133E-07	477.
17047–2848	355.4	6.9	14.8	-6.2	7.76	-5.22	3.95	0.137E-04	0.247E-07	553.
17050–4642	341.2	-3.9	11.7	-41.1	8.28	-5.39	5.44	0.642E-05	0.466E-07	138.
17079–6554	325.5	-15.4	14.8	-46.8	5.71	-5.01	1.40	0.391E-05	0.103E-07	379.
17155–4917	340.1	-6.8	24.2	-71.8	8.31	-5.20	5.02	0.191E-04	0.454E-07	422.
17209–3318	353.8	1.5	x	-41.0	7.39	-5.29	3.44	x	x	x
17222–2328	2.1	6.8	17.4	-60.2	7.67	-5.25	3.84	0.241E-04	0.339E-07	710.
17278–3937	349.3	-3.2	27.7	-33.3	7.56	-5.04	3.32	0.682E-05	0.354E-07	193.
17309–3412	354.2	-0.8	16.8	-32.8	8.28	-5.32	5.24	0.156E-04	0.673E-07	232.
17375–3652	352.7	-3.3	22.5	-24.8	6.53	-5.58	2.65	0.429E-04	0.144E-06	299.
17547–3249	358.0	-4.3	12.0	45.5	8.48	-5.38	5.90	0.107E-04	0.519E-07	206.
17556+5813	86.8	29.9	16.8	-14.5	4.89	-4.78	0.86	0.242E-05	0.618E-08	392.
17599–4556	346.9	-11.5	11.9	42.1	8.42	-5.11	5.08	0.253E-05	0.128E-07	197.
18030–1705	12.6	1.9	17.4	0.9	8.44	-5.17	5.27	0.133E-04	0.378E-07	351.
18082–2454	6.4	-2.9	x	22.7	7.27	-5.11	2.98	x	x	x
18092–0437	24.3	6.7	29.8	-27.7	6.40	-5.30	2.19	0.337E-05	0.751E-07	45.
18147–2215	9.4	-3.0	20.9	0.6	7.36	-5.30	3.40	0.231E-04	0.639E-07	362.
18230+0544	35.1	8.4	15.0	49.7	6.63	-5.01	2.13	0.756E-05	0.131E-07	579.
18234–2204	10.5	-4.7	23.8	10.6	7.04	-5.27	2.90	0.131E-04	0.908E-07	145.
18244–0104	29.1	4.9	16.8	43.3	7.57	-4.98	3.23	0.464E-05	0.811E-08	572.
18276–4717	347.7	-16.4	18.3	14.5	4.71	-4.96	0.86	0.370E-05	0.646E-08	573.
18356–0951	22.7	-1.6	28.2	70.8	7.37	-5.13	3.16	0.143E-04	0.337E-07	423.
19008+0726	41.0	0.8	28.4	14.5	4.75	-5.13	0.95	0.114E-04	0.221E-07	515.
19029+2017	52.6	6.3	21.1	39.8	6.98	-5.10	2.60	0.918E-05	0.275E-07	334.
19108+1155	46.1	0.7	26.6	67.8	7.42	-5.00	3.05	0.129E-04	0.184E-07	698.
19136+6727	98.6	22.9	11.1	-23.0	8.22	-5.06	4.52	0.906E-06	0.135E-07	67.
19238+1159	47.6	-2.0	16.2	65.0	7.47	-5.45	3.83	0.797E-05	0.974E-07	82.
19248+0658	43.3	-4.7	16.1	-1.5	6.57	-4.95	2.02	0.490E-05	0.115E-07	426.
19253+1918	54.2	1.1	25.0	42.0	8.42	-5.30	5.54	0.235E-04	0.946E-07	248.
19276–0056	36.6	-9.0	26.7	24.0	7.20	-4.87	2.59	0.657E-05	0.255E-07	257.
19285+1805	53.6	-0.1	25.3	55.4	7.72	-5.26	3.95	x	x	x
19289+1931	54.8	0.5	x	18.0	7.45	-5.08	3.20	x	x	x
19296+2227	57.5	1.8	11.4	39.9	8.03	-5.51	5.10	0.122E-04	0.833E-07	146.
19304+2529	60.2	3.1	16.5	47.1	7.86	-5.52	4.73	0.154E-05	0.123E-06	13.
19358+0917	46.7	-5.9	17.4	21.5	7.58	-5.21	3.62	0.244E-05	0.406E-07	60.
19381+3315	67.8	5.4	15.2	50.8	7.12	-5.02	2.67	0.264E-05	0.121E-07	217.
19417+3053	66.2	3.6	18.8	11.6	8.26	-5.29	5.15	0.102E-04	0.438E-07	232.
19419+3222	67.5	4.3	19.4	21.0	7.83	-5.10	3.85	0.387E-05	0.135E-07	287.
19455+0920	47.9	-8.0	14.6	49.3	7.17	-5.14	2.90	0.814E-05	0.205E-07	396.
19455+2319	60.0	-1.0	x	38.0	8.17	-5.21	4.74	x	x	x
19457+2346	60.5	-0.8	19.3	22.0	7.77	-5.18	3.89	0.236E-04	0.358E-07	658.
19485+3235	68.4	3.2	20.5	25.5	8.08	-5.26	4.66	0.248E-04	0.373E-07	666.
19523+2414	61.6	-1.8	22.2	7.6	8.44	-5.14	5.20	0.289E-04	0.323E-07	894.
19524+2130	59.3	-3.3	21.2	28.2	8.54	-5.16	5.50	0.225E-04	0.313E-07	719.
19537+2212	60.1	-3.2	15.1	23.5	5.92	-4.92	1.47	0.186E-05	0.599E-08	310.
19552+3142	68.3	1.5	27.2	-4.0	7.91	-5.22	4.21	0.123E-04	0.514E-07	239.
19558+3333	70.0	2.4	19.2	8.0	7.70	-5.43	4.22	0.190E-04	0.879E-07	216.
19559+3303	69.5	2.1	18.6	38.0	8.27	-5.03	4.57	0.990E-05	0.381E-07	260.
20004+2943	67.2	-0.5	35.4	18.0	7.24	-4.96	2.76	x	x	x
20014+2830	66.3	-1.3	22.4	17.1	8.32	-5.26	5.21	0.274E-04	0.656E-07	418.

Table 1. continued.

IRAS Name	l	b	v_e (km s ⁻¹)	v_{LSR} (km s ⁻¹)	m_{bol} (mag)	M_{bol} (mag)	d (kpc)	\dot{M}_g (M_{\odot} yr ⁻¹)	\dot{M}_d (M_{\odot} yr ⁻¹)	\dot{M}_g/\dot{M}_d
20082+3228	70.5	-0.4	x	16.0	7.45	-5.18	3.35	x	x	x
20084-1425	28.6	-24.0	10.6	3.3	7.70	-4.99	3.45	0.149E-05	0.602E-08	248.
20159+3134	70.6	-2.2	28.3	4.0	8.45	-5.15	5.24	0.648E-04	0.438E-07	1479.
20171+3519	73.9	-0.3	x	-16.7	7.35	-5.29	3.36	x	x	x
20200+3624	75.1	-0.2	23.5	14.3	7.91	-5.08	3.96	0.118E-04	0.427E-07	277.
20204+2914	69.3	-4.4	15.8	15.4	7.84	-5.16	3.97	0.144E-04	0.263E-07	548.
20253+3814	77.2	0.0	26.2	-7.1	7.79	-5.24	4.04	x	x	x
20277+2958	70.8	-5.2	17.0	6.6	8.51	-5.34	5.88	0.187E-04	0.408E-07	459.
20282+3605	75.8	-1.7	18.2	0.8	7.56	-5.06	3.35	0.155E-05	0.271E-07	57.
20323+3153	72.9	-4.9	14.0	59.5	7.84	-5.18	4.01	0.273E-05	0.284E-07	96.
20331+4621	84.6	3.7	x	25.0	6.92	-5.17	2.62	x	x	x
20396+4757	86.5	3.8	15.5	14.3	3.84	-4.78	0.53	0.247E-05	0.679E-08	364.
20461+4817	87.5	3.1	31.2	-41.4	8.55	-5.20	5.64	0.600E-04	0.549E-07	1093.
20546+6401	100.6	12.2	14.6	-7.1	8.41	-5.05	4.94	0.154E-04	0.139E-07	1109.
20564+1857	65.8	-17.1	10.5	7.4	8.06	-4.99	4.07	0.258E-05	0.616E-08	419.
20596+3833	81.6	-5.0	27.4	19.4	7.92	-5.09	4.00	0.216E-04	0.323E-07	669.
21006+4720	88.3	0.7	x	-2.0	6.74	-5.02	2.25	x	x	x
21027+3702	80.9	-6.5	15.2	-6.7	6.47	-5.03	2.00	0.730E-06	0.125E-07	58.
21070+4711	88.9	-0.2	21.1	-22.0	7.51	-5.05	3.26	0.683E-05	0.112E-07	612.
21088+4546	88.1	-1.4	18.9	-45.2	7.99	-5.03	4.02	0.830E-05	0.132E-07	630.
21197-6956	323.2	-38.2	9.9	-3.1	6.48	-5.00	1.97	0.283E-05	0.815E-08	347.
21262+7005	107.2	13.9	14.4	13.3	6.51	-4.71	1.75	0.536E-05	0.691E-08	776.
21265+5042	93.7	0.0	23.2	-18.7	8.64	-5.10	5.61	0.244E-04	0.355E-07	687.
21324+5537	97.7	3.0	20.5	-36.0	7.78	-5.31	4.15	0.401E-04	0.571E-07	703.
21366+4529	91.4	-5.0	20.2	32.4	6.86	-4.96	2.31	0.534E-05	0.957E-08	557.
21377+5042	95.0	-1.2	18.0	-7.5	6.83	-4.97	2.29	0.491E-05	0.170E-07	288.
21383+4513	91.5	-5.4	31.9	-21.5	6.96	-5.13	2.61	0.100E-04	0.237E-07	422.
21424+5821	100.5	4.1	25.7	-31.5	7.91	-5.03	3.87	0.164E-04	0.209E-07	783.
21444+5053	95.9	-1.8	12.9	-47.6	8.69	-5.36	6.48	0.350E-04	0.383E-07	913.
22039+5328	99.9	-1.6	36.3	-41.0	7.15	-4.98	2.66	0.330E-05	0.995E-08	332.
22236+5002	100.5	-6.1	22.3	-32.0	7.88	-5.05	3.84	0.233E-04	0.211E-07	1101.
23174+6810	114.6	7.1	16.5	-17.8	8.16	-5.23	4.74	0.583E-04	0.507E-07	1150.
23234+6434	114.0	3.5	18.6	-37.1	8.45	-5.43	5.96	0.832E-04	0.886E-07	939.
23491+6243	116.2	0.9	21.7	-4.2	7.72	-5.13	3.71	0.196E-04	0.493E-07	397.
23516+6430	116.9	2.6	18.1	-62.5	7.73	-5.29	4.02	0.202E-04	0.550E-07	367.
00210+6221	119.8	-0.1	x	-38.0	7.57	-5.43	3.97	x	x	x
00247+6922	120.9	6.9	17.2	-27.7	5.48	-5.27	1.41	0.114E-04	0.231E-07	495.
01133+2530	129.9	-36.8	3.5	13.0	6.82	-4.96	2.26	0.440E-06	0.344E-08	128.
01142+6306	125.9	0.6	14.0	-21.0	8.07	-5.19	4.49	0.205E-04	0.244E-07	842.
01144+6658	125.5	4.5	18.0	-39.3	6.42	-5.82	2.79	0.638E-04	0.151E-06	424.
02152+2822	145.0	-30.5	9.5	-2.0	6.58	-5.22	2.29	0.298E-05	0.418E-07	71.
02293+5748	136.1	-2.2	14.2	7.0	6.18	-5.37	2.04	0.228E-04	0.531E-07	430.
03112-5730	273.3	-50.9	5.3	1.0	6.36	-5.02	1.89	0.829E-06	0.589E-08	141.
03186+7016	135.1	11.3	7.8	-15.9	6.36	-5.11	1.97	0.577E-05	0.195E-07	296.
03229+4721	148.2	-7.6	15.9	-16.2	4.31	-5.05	0.74	0.545E-05	0.933E-08	584.
03301+5658	143.6	1.0	17.0	-46.0	8.83	-5.39	6.98	0.284E-04	0.645E-07	441.
03313+6058	141.5	4.3	13.9	-39.0	8.06	-5.54	5.24	0.237E-04	0.114E-06	208.
03448+4432	152.9	-7.6	13.3	-23.0	6.49	-5.27	2.25	0.964E-05	0.345E-07	279.
04307+6210	146.0	9.9	15.0	-45.0	5.07	-4.99	1.03	0.739E-05	0.728E-08	1014.
04340+4623	158.0	-0.4	16.0	25.0	7.81	-5.31	4.22	0.174E-04	0.514E-07	339.
04530+4427	161.6	0.9	19.6	14.0	6.78	-5.30	2.60	0.289E-04	0.542E-07	533.
05104+2055	182.7	-10.4	25.2	13.0	6.09	-4.98	1.64	0.830E-05	0.133E-07	625.
05136+4712	161.6	5.4	14.7	-44.0	7.32	-5.08	3.02	0.140E-04	0.161E-07	867.
05405+3240	176.6	1.6	26.0	-31.0	6.04	-5.47	2.01	0.796E-04	0.675E-07	1180.
05418-3224	237.2	-27.6	10.0	24.0	8.17	-5.00	4.31	0.107E-04	0.665E-08	1612.
05426+2040	187.1	-4.3	11.8	15.0	5.51	-4.98	1.25	0.117E-05	0.837E-08	140.

Table 1. continued.

IRAS Name	l	b	v_e (km s ⁻¹)	v_{LSR} (km s ⁻¹)	m_{bol} (mag)	M_{bol} (mag)	d (kpc)	\dot{M}_g (M_{\odot} yr ⁻¹)	\dot{M}_d (M_{\odot} yr ⁻¹)	\dot{M}_g/\dot{M}_d
06012+0726	200.8	-7.0	16.6	43.3	5.51	-5.33	1.47	0.181E-04	0.436E-07	415.
06192+4657	167.5	14.9	7.7	-23.0	7.76	-5.27	4.03	0.863E-05	0.199E-07	434.
06206+0931	201.3	-1.8	10.0	12.0	7.51	-5.03	3.22	0.265E-05	0.100E-07	264.
06230-0930	218.6	-10.1	12.9	25.0	6.75	-4.96	2.19	0.635E-05	0.111E-07	575.
06238+0904	202.1	-1.3	16.0	35.0	7.80	-5.13	3.86	0.132E-04	0.281E-07	469.
06268+0849	202.6	-0.8	33.0	35.0	7.46	-5.17	3.36	0.255E-04	0.545E-07	468.
06291+4319	171.6	15.1	21.4	-39.0	6.60	-5.10	2.19	0.105E-04	0.215E-07	487.
06342+0328	208.2	-1.7	9.0	1.0	5.62	-5.27	1.51	0.612E-05	0.140E-07	439.
06487+0551	207.8	2.6	11.0	29.0	7.00	-5.06	2.59	0.169E-05	0.147E-07	115.
06505-0450	217.5	-1.9	12.0	53.0	8.25	-5.25	5.00	0.118E-04	0.302E-07	393.
06564+0342	210.6	3.4	9.9	31.0	7.59	-5.12	3.49	0.103E-04	0.170E-07	607.
06582+1507	200.5	8.9	13.7	22.0	7.81	-5.55	4.70	0.143E-04	0.107E-06	134.
07057-1150	225.4	-1.8	11.7	0.0	7.53	-5.05	3.27	0.710E-05	0.118E-07	604.
07065-7256	284.2	-24.8	21.2	-3.0	5.34	-4.86	1.10	0.225E-05	0.108E-07	209.
07098-2012	233.3	-4.8	23.8	9.0	5.72	-5.39	1.66	0.141E-04	0.262E-07	539.
07203-3212	245.1	-8.2	13.0	43.0	7.73	-5.14	3.75	0.131E-04	0.193E-07	679.
07217-1246	228.1	1.2	24.9	21.0	6.32	-5.03	1.86	0.483E-05	0.196E-07	246.
07434-1847	235.9	2.8	14.0	60.0	8.33	-5.29	5.29	0.127E-04	0.360E-07	352.
07454-7112	283.4	-21.5	13.5	-36.5	4.74	-5.12	0.94	0.162E-04	0.188E-07	864.
07576-4054	256.5	-5.9	7.0	4.0	7.18	-5.18	2.96	0.328E-05	0.159E-07	205.
07582-1933	238.4	5.4	14.6	6.0	6.96	-5.15	2.65	0.723E-05	0.221E-07	328.
08045-1524	235.6	8.9	13.7	-22.0	7.25	-5.04	2.87	0.322E-05	0.117E-07	275.
08050-2838	246.9	1.9	15.0	-11.0	6.95	-5.08	2.55	0.121E-04	0.161E-07	752.
08074-3615	253.5	-1.8	21.7	9.8	6.30	-5.31	2.10	0.330E-04	0.671E-07	492.
08088-3243	250.7	0.4	20.7	-21.0	5.25	-5.12	1.19	0.196E-04	0.214E-07	916.
08171-2134	242.5	8.1	16.3	-9.0	6.59	-5.43	2.53	0.389E-04	0.812E-07	479.
08191-3653	255.4	-0.2	18.0	85.0	7.87	-5.30	4.31	0.229E-04	0.495E-07	462.
09116-2439	252.8	16.2	12.8	0.0	4.57	-5.30	0.94	0.131E-04	0.216E-07	607.
09452+1330	221.4	45.1	15.4	-25.5	0.00	-5.23	0.11	0.150E-04	0.245E-07	612.
09513-5324	278.3	0.5	20.0	-9.0	6.28	-5.20	1.97	0.202E-04	0.362E-07	557.
09521-7508	292.3	-16.4	12.8	-4.0	5.39	-5.14	1.28	0.109E-04	0.182E-07	600.
10131+3049	197.7	56.0	17.5	-1.6	2.29	-5.25	0.32	0.192E-05	0.136E-07	141.
10350-1307	260.0	38.1	10.7	-30.0	5.11	-4.85	0.98	0.440E-05	0.540E-08	814.
10491-2059	269.0	33.6	28.5	-14.0	3.87	-5.04	0.60	0.831E-05	0.254E-07	328.
11145-6534	293.4	-4.7	18.5	-24.0	6.12	-5.19	1.83	0.166E-04	0.342E-07	484.
11308-1020	273.7	47.8	11.0	20.0	6.85	-5.01	2.35	0.348E-05	0.876E-08	397.
11318-7256	297.3	-11.2	26.5	-2.0	4.32	-4.96	0.72	0.575E-05	0.847E-08	679.
12394-4338	301.2	18.9	16.1	-32.0	6.09	-5.07	1.71	0.889E-05	0.170E-07	524.
12540-6845	303.5	-6.2	28.8	-35.0	5.66	-5.13	1.44	0.284E-04	0.437E-07	650.
14484-6152	316.6	-2.5	19.0	24.4	3.81	-4.98	0.57	0.392E-05	0.110E-07	357.
15082-4808	325.6	8.3	20.4	-3.0	4.49	-5.15	0.85	0.276E-04	0.318E-07	868.
15084-5702	321.1	0.6	26.0	-44.0	6.84	-5.35	2.75	0.177E-04	0.101E-06	175.
15148-4940	325.8	6.4	26.9	-43.0	5.30	-4.99	1.14	0.914E-05	0.129E-07	706.
15194-5115	325.5	4.7	22.2	-15.0	3.73	-5.14	0.59	0.181E-04	0.263E-07	688.
16079-4812	333.6	2.3	14.5	-42.6	6.33	-5.27	2.08	0.226E-04	0.369E-07	611.
17049-2440	358.8	9.3	20.5	-4.1	4.52	-5.46	0.99	0.954E-05	0.505E-07	189.
17079-3243	352.7	4.0	25.6	21.0	5.89	-5.06	1.55	0.149E-04	0.270E-07	551.
17389-5742	334.7	-14.3	16.0	19.0	5.71	-4.97	1.37	0.467E-05	0.868E-08	538.
17446-4048	350.1	-6.6	16.7	2.0	5.72	-5.13	1.48	0.153E-04	0.194E-07	786.
17446-7809	315.4	-23.6	15.9	-1.0	5.06	-5.08	1.07	0.756E-05	0.184E-07	411.
17534-3030	359.9	-2.9	19.0	-8.0	6.05	-5.46	2.00	0.376E-04	0.106E-06	356.
17581-1744	11.5	2.6	17.8	25.0	7.19	-5.08	2.85	0.889E-05	0.224E-07	397.
18036-2344	6.9	-1.5	21.7	22.7	6.53	-5.23	2.25	0.309E-04	0.510E-07	605.
18040-0941	19.2	5.3	28.4	30.0	5.56	-5.03	1.31	0.183E-04	0.241E-07	758.
18119-2244	8.7	-2.7	17.8	22.7	6.74	-5.21	2.45	0.822E-05	0.408E-07	201.
18156-0653	23.0	4.2	20.0	23.7	5.95	-5.19	1.69	0.662E-05	0.105E-07	629.
18194-2708	5.6	-6.2	23.0	48.0	4.19	-5.33	0.80	0.767E-05	0.233E-07	330.

Table 1. continued.

IRAS Name	l	b	v_e (km s ⁻¹)	v_{LSR} (km s ⁻¹)	m_{bol} (mag)	M_{bol} (mag)	d (kpc)	\dot{M}_g (M_{\odot} yr ⁻¹)	\dot{M}_d (M_{\odot} yr ⁻¹)	\dot{M}_g/\dot{M}_d
18239–0655	24.0	2.3	28.0	0.0	5.90	-5.18	1.64	0.516E-05	0.555E-07	93.
18240+2326	51.6	15.8	15.1	60.0	4.61	-5.20	0.92	0.456E-05	0.288E-07	158.
18244–0815	22.8	1.6	20.0	48.0	7.78	-5.19	3.93	0.160E-04	0.374E-07	428.
18248–0839	22.5	1.3	16.1	31.0	6.31	-5.30	2.10	0.357E-05	0.480E-07	75.
18269–1257	19.0	-1.1	14.0	70.0	7.14	-5.29	3.06	0.475E-05	0.464E-07	102.
18306+3657	65.3	19.5	26.0	14.0	5.74	-4.96	1.38	0.346E-05	0.789E-08	439.
18320–0352	27.6	2.0	22.0	64.0	7.39	-5.43	3.67	0.273E-04	0.821E-07	332.
18369–1034	22.2	-2.2	13.0	41.0	8.05	-5.33	4.75	0.140E-04	0.457E-07	307.
18397+1738	47.8	10.0	13.4	0.0	4.79	-4.99	0.90	0.487E-05	0.183E-07	266.
18398–0220	29.9	1.0	36.0	3.0	4.70	-5.18	0.95	x	x	x
18400–0704	25.7	-1.3	17.0	148.0	8.00	-5.30	4.57	0.100E-04	0.508E-07	197.
18424+0346	35.6	3.2	20.0	8.0	7.40	-5.11	3.17	0.145E-04	0.311E-07	465.
18464–0656	26.5	-2.6	15.4	59.8	6.97	-5.37	2.94	0.462E-05	0.599E-07	77.
18475+0926	41.2	4.7	21.8	22.0	5.88	-5.17	1.62	0.168E-04	0.337E-07	499.
19029+0808	41.8	0.7	17.0	2.0	7.01	-5.30	2.90	0.147E-04	0.567E-07	259.
19068+0544	40.1	-1.3	20.5	65.0	7.47	-5.09	3.25	0.369E-04	0.368E-07	1001.
19175–0807	29.0	-10.0	22.5	21.0	5.25	-5.31	1.29	0.171E-04	0.387E-07	443.
19321+2757	62.6	4.0	24.4	-12.0	5.45	-5.22	1.36	0.383E-04	0.380E-07	1008.
19346+1209	49.1	-4.3	14.5	73.0	8.11	-5.18	4.57	0.237E-04	0.300E-07	790.
19548+3035	67.3	1.0	22.3	5.7	7.09	-5.55	3.38	0.114E-03	0.215E-06	532.
19594+4047	76.5	5.6	20.5	29.5	5.45	-5.47	1.53	0.249E-04	0.572E-07	436.
20072+3116	69.4	-0.9	25.6	17.8	6.15	-5.08	1.76	0.205E-04	0.454E-07	453.
20311+4222	81.2	1.6	13.1	24.9	6.52	-5.14	2.15	0.487E-05	0.185E-07	263.
20435+3825	79.5	-2.7	20.6	0.0	6.28	-5.12	1.90	0.319E-05	0.323E-07	99.
20532+5554	94.1	7.1	11.4	2.0	7.36	-5.16	3.19	0.960E-05	0.302E-07	317.
20570+2714	72.6	-12.0	23.5	1.0	5.62	-5.43	1.62	0.241E-04	0.392E-07	615.
21003+4801	88.8	1.1	14.8	-5.0	6.84	-5.25	2.62	0.115E-04	0.331E-07	347.
21032–0024	49.6	-29.6	16.1	1.0	4.97	-4.86	0.92	0.490E-05	0.885E-08	554.
21035+5136	91.8	3.2	11.4	7.0	5.53	-5.04	1.30	0.398E-05	0.121E-07	329.
21147+5110	92.7	1.6	11.5	-49.0	7.23	-5.27	3.17	0.150E-04	0.319E-07	470.
21318+5631	98.2	3.7	19.6	1.7	5.76	-5.48	1.77	0.769E-05	0.118E-06	65.
21320+3850	86.3	-9.4	13.0	-5.0	5.05	-4.90	0.98	0.378E-05	0.756E-08	500.
21358+7823	113.8	19.4	22.5	-15.5	4.35	-4.94	0.72	0.341E-05	0.947E-08	360.
21373+4540	91.6	-5.0	14.7	-21.0	6.61	-5.17	2.27	0.902E-05	0.264E-07	342.
21449+4950	95.3	-2.6	14.6	-30.0	7.21	-5.26	3.11	0.892E-05	0.285E-07	313.
21489+5301	97.8	-0.6	22.3	-28.0	6.67	-5.33	2.51	0.592E-04	0.763E-07	776.
22241+6005	105.8	2.4	34.2	-6.0	6.11	-5.35	1.96	0.711E-04	0.662E-07	1074.
22303+5950	106.4	1.8	18.3	-65.0	7.44	-5.49	3.86	0.319E-04	0.109E-06	294.
22354+5911	106.6	0.9	21.0	-40.0	8.87	-5.18	6.44	0.277E-04	0.478E-07	579.
22518+6600	111.5	6.1	19.2	-22.0	6.73	-5.04	2.27	0.852E-05	0.205E-07	416.
22585+6402	111.3	4.0	21.4	-5.0	6.78	-5.10	2.37	0.574E-04	0.283E-07	2026.
23166+1655	93.5	-40.4	15.1	-30.8	4.66	-5.35	1.00	0.144E-04	0.827E-07	174.
23174+5941	111.7	-0.9	15.0	-55.0	8.23	-5.08	4.58	0.716E-05	0.166E-07	430.
23257+1038	92.2	-46.9	10.5	47.0	6.08	-4.96	1.61	0.847E-05	0.226E-07	374.
23279+5336	111.0	-7.1	8.8	-32.0	7.12	-5.11	2.78	0.259E-05	0.138E-07	187.
23320+4316	108.5	-17.1	14.7	-17.0	4.24	-5.23	0.78	0.704E-05	0.244E-07	288.

Figure 3 (left-hand panel) shows the distribution of M_{bol} as a function of galactic longitude. The mean absolute bolometric magnitude is -5.16 with a dispersion of 0.16 magnitudes considering all 310 objects. A quadratic fit is made to M_{bol} as a function of Galactic longitude, with outliers at the 2.5σ level removed, but the linear and quadratic term are found to be not significant. Considering clipping at the 2.5σ level and a constant M_{bol} , the best estimate remains -5.16 ± 0.16 mag using 307 stars.

3.3. Mass loss rates

The gas mass loss rate will be derived from the CO line. From Olofsson (1993),

$$\dot{M}_g = 1.4 \times \frac{T_{\text{mb}} v_e^2 D^2 B^2}{2 \times 10^{19} J_{\text{CO}}^{0.85} s(J)}, \quad (3)$$

is used, where \dot{M}_g is in solar masses per year, T_{mb} is the main-beam peak temperature in Kelvin, v_e is the gas expansion

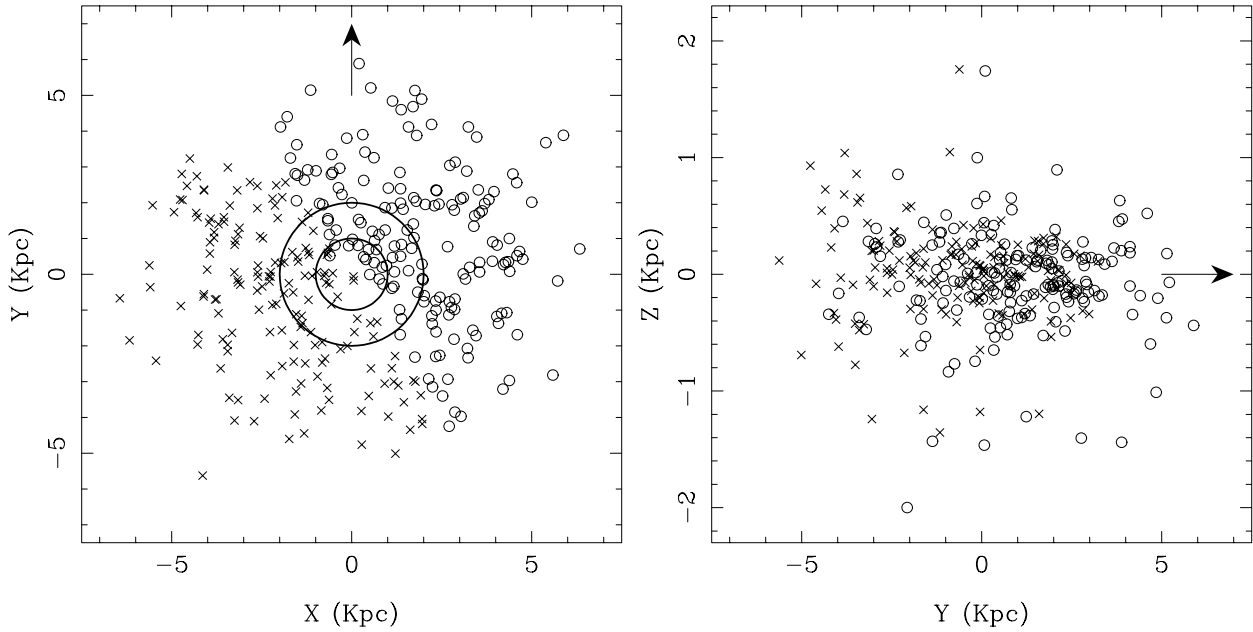


Fig. 2. Projection of the objects onto the planes $Z = 0$ (left panel) and $X = 0$ (right panel). The circles in the left-hand panel indicate 1 and 2 kpc distance to the Sun. The arrow points to the Galactic centre which is located at $Y = +8.5$, $X = Z = 0$. Sources with $\delta < 0$ (> 0) are indicated by the open circles (crosses).

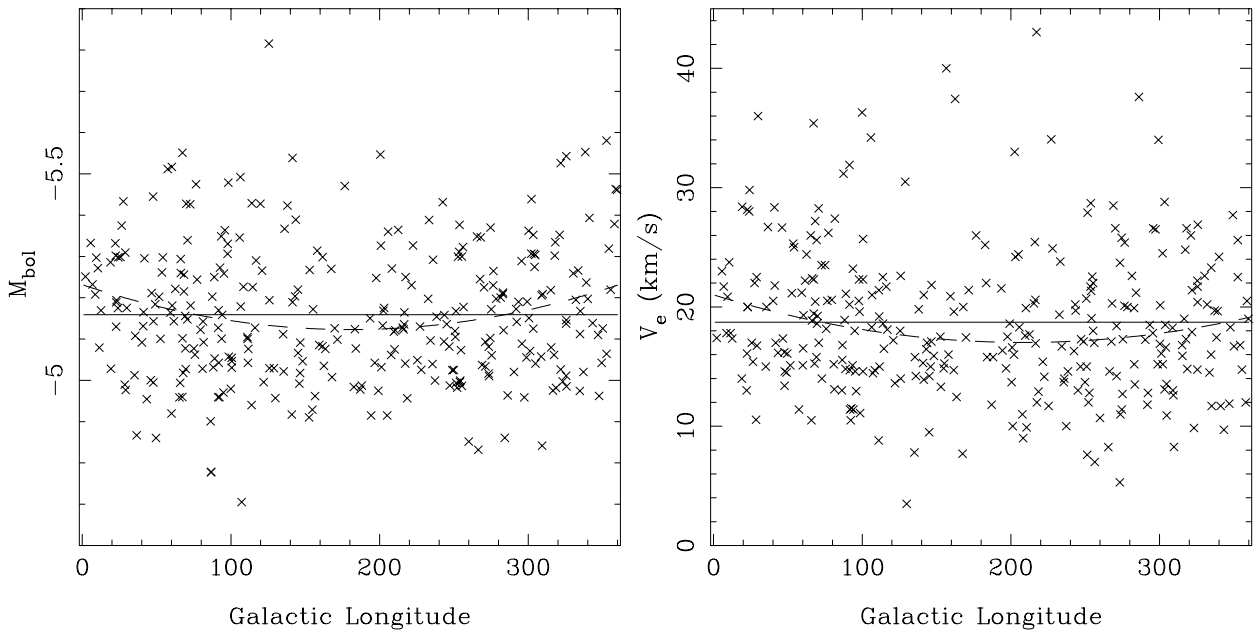


Fig. 3. Bolometric magnitude, M_{bol} , and expansion velocity, v_e , plotted versus galactic longitude. Linear (solid line) and quadratic (dashed line) fits to the data are indicated (see text).

velocity in km s^{-1} , D is the distance in parsec, B is the FWHM size of the telescope beam in arcsec, f_{CO} is the CO abundance relative to H_2 , and $s(J)$ is a correction factor, equal to unity for the $J = 1-0$ transition and 0.6 for the $J = 2-1$ transition.

The dust mass loss rate will be derived from the IRAS $60 \mu\text{m}$ flux. From Jura (1988; also see Groenewegen et al. 1998b, 1999),

$$\dot{M}_d = C v_{d,15} D^2 L_4^{-0.5} \lambda_{10}^{0.5} \kappa_{150}^{-1} F(\lambda) \quad (4)$$

is used, where \dot{M}_d is in solar masses per year, C is a constant, $v_{d,15}$ is the dust expansion velocity in units of 15 km s^{-1} , D is the distance in kpc, L_4 is the luminosity in units of $10\,000 L_{\odot}$, λ_{10} is the wavelength in units of $10 \mu\text{m}$ where the peak of the energy distribution occurs, κ_{150} is the opacity at $60 \mu\text{m}$ in units of $150 \text{ cm}^2 \text{g}^{-1}$, and $F(\lambda)$ is the circumstellar emission at $60 \mu\text{m}$ in Jansky.

Given the red colours of the objects under consideration, the stellar contribution to the observed $60 \mu\text{m}$ flux can be neglected (Groenewegen et al. 1998b) and the observed flux can

be entirely contributed to dust emission. From detailed modelling in Groenewegen et al. (1999), a constant $C = 5.35 \times 10^{-10}$ for carbon stars is used.

The dust expansion velocity is calculated from $v_d = v_g + v_{dr}$, with the drift velocity calculated from (e.g. Groenewegen et al. 1998b):

$$v_{dr} = 1.43 \times 10^{-4} \times \sqrt{\frac{Q_F L v_c}{\dot{M}_g}} \quad (\text{km s}^{-1}), \quad (5)$$

where Q_F is the flux-averaged absorption coefficient.

The formalism to calculate the mass loss rates is used here with $f_{\text{CO}} = 8 \times 10^{-4}$ (e.g. Olofsson 1993), $\kappa_{150} = 1$, $\lambda_{10} = 0.3$ (typical for the infrared stars studied in Groenewegen et al. 1998b) and $Q_F = 0.025$ (the average of values in Groenewegen et al. 1998b). Typical values for the drift velocity are 2–3 km s⁻¹.

Figure 4 shows the distribution of gas- and dust mass loss rate, and gas-to-dust ratio as a function of galactic longitude. Quadratic fits as a function of Galactic longitude are made, but the linear and quadratic terms are found to be not significant. The average gas mass loss rate is $1.1 \times 10^{-5} M_{\odot} \text{ yr}^{-1}$, the average dust mass loss rate is $2.7 \times 10^{-8} M_{\odot} \text{ yr}^{-1}$ and the average gas-to-dust ratio is 400, all based on 304 objects.

The spread in the gas-to-dust ratio is almost a factor of 15, and this may seem surprisingly high. As the gas-to-dust ratio is derived from dividing the gas and dust mass loss rate, any scatter due to the approximative nature of both formula themselves, as well as intrinsic scatter in the quantities assumed constant in these formula (the CO abundance, the dust opacity, the peak wavelength of the SED), will contribute to the scatter in the gas-to-dust ratio. A factor of 2 scatter in each of these quantities will already lead to a scatter of 5 in the derived gas-to-dust ratio, indicating that the “cosmic” scatter in the gas-to-dust ratio (due to differences in the amount of condensable material available, and the efficiency of dust condensation) is about a factor of three. Radiation-hydrodynamical models from the Berlin and Vienna groups for the atmospheres and circumstellar shells of carbon-rich long-period variables which include dust formation calculate, time- and spatial averaged, gas-to-dust ratios. Forty-four selected models from Fleischer et al. (1992), Arndt et al. (1997) and Höfner & Dorfi (1997), as outlined in Groenewegen et al. (1998b), have an average gas-to-dust ratio of 300 with 90% of values being in the range 200 to 700. The conclusion is that most of the scatter observed in the gas-to-dust ratio in the bottom panel of Fig. 4 is due to scatter in the gas- and dust mass loss rates, and that the remaining scatter of about a factor of three is in good agreement with the scatter predicted by radiation-hydrodynamical models due to variations in the stellar parameters (mass, effective temperature, luminosity, C/O ratio, pulsation period). The observed mean gas-to-dust ratio is in good agreement with theory.

3.4. The expansion velocity

The mean velocity over all stars is 18.7 km s⁻¹, with a dispersion of 6.1 km s⁻¹. A quadratic fit is made to the velocity as a function of Galactic longitude. The rms is determined and the

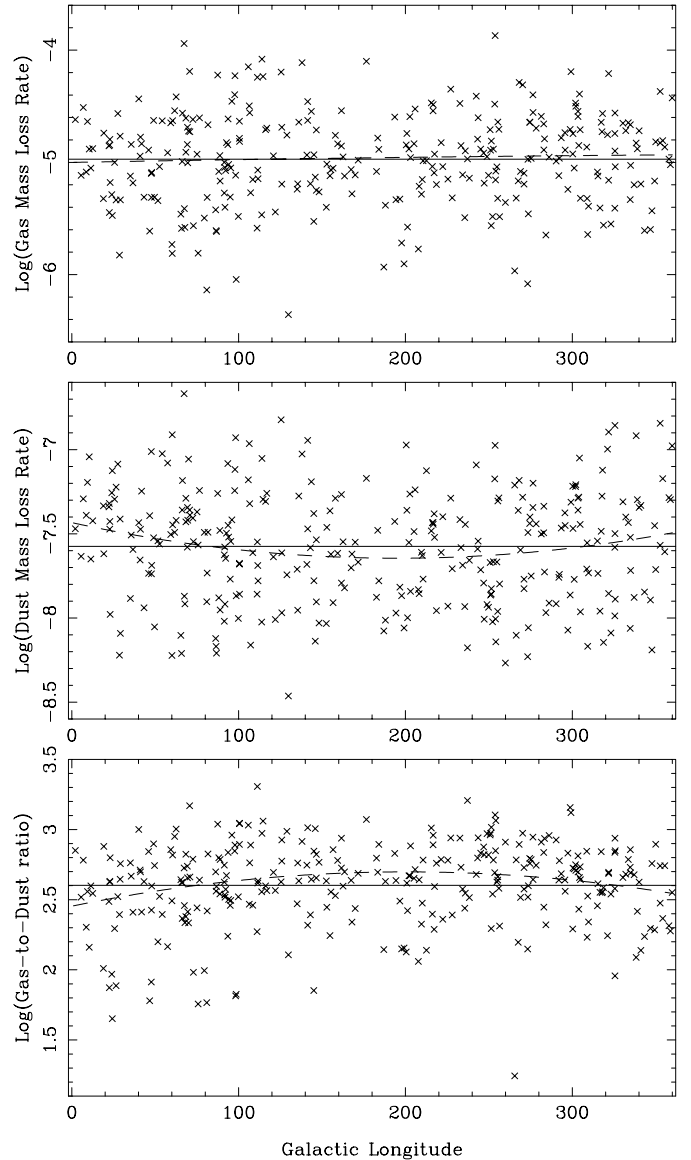


Fig. 4. Gas and dust mass loss rate, and gas-to-dust ratio versus galactic longitude. Linear (solid line) and quadratic (dashed line) fits are indicated.

10 objects that deviate by more than 2.5σ are removed. The final fit is:

$$v_e = 17.09(\pm 0.09) - 5.27(\pm 0.55) \times 10^{-3} (l - 180) + 9.48(\pm 0.65) \times 10^{-5} (l - 180)^2, \quad (6)$$

with a rms of 5.2 km s⁻¹, based on 299 stars. The data and the fit are shown in the right-hand panel of Fig. 3.

3.5. Replenishment of the ISM

The number of objects in a cylinder centred on the Sun perpendicular to the Galactic plane, with a radius of 0.75, 1, 1.5, 2 and 3 kpc, respectively, is determined and their gas and dust mass loss rates summed. The results are listed in Table 2. For a limiting distance (much) greater than the scale height the number of objects is expected to vary with the square of the limiting

Table 2. Replenishment of the ISM by infrared carbon stars.

Limiting projected distance (kpc)	N	Dust ($M_{\odot} \text{ yr}^{-1}$)	Gas ($M_{\odot} \text{ yr}^{-1}$)
<0.75	11	1.65E-7	7.37E-5
<1.0	26	5.21E-7	2.10E-4
<1.5	47	9.14E-7	4.49E-4
<2.0	77	1.79E-6	7.81E-4
<3.0	143	4.16E-6	1.75E-3

distance in a complete sample. This is approximately true up to 1.5 kpc. Based on this limiting distance, the surface density of the sample is then calculated to be $6.6 \pm 1.0 \text{ kpc}^{-2}$ (the error is based on Poisson statistics), and the rate of replenishment $1.3 \times 10^{-7} M_{\odot} \text{ yr}^{-1} \text{ kpc}^{-2}$ in dust and $6.3 \times 10^{-5} M_{\odot} \text{ yr}^{-1} \text{ kpc}^{-2}$ in gas. This is slightly less, but within the uncertainties, of the rate of $2.3 \times 10^{-4} M_{\odot} \text{ yr}^{-1} \text{ kpc}^{-2}$, calculated in Olivier et al. (2001) for a sample of 58 nearby O- and C-rich dust enshrouded AGB stars, considering that about half of the stars in their sample are carbon rich.

4. Discussion

An analysis of the distribution, expansion velocity and gas & dust mass loss rate of a sample of about 300 infra-red carbon stars is presented.

Based on Fig. 2 we show that the surface density of (infra-red) carbon stars is essentially constant in the solar neighbourhood, in agreement with earlier studies (Jura 1991; Groenewegen et al. 1992; Guglielmo et al. 1998), and in disagreement with the recent suggestion of Le Bertre et al. (2001; hereafter LeBe2001) that there is a “clear preference” for carbon stars to be located outside the solar circle. The surface density is found to be $6.6 \pm 1.0 \text{ kpc}^{-2}$.

Recently, LeBe2001 analysed a sample of mass losing AGB stars detected with the Japanese IRTS telescope, and it is instructive to compare distances and mass loss rates derived in a completely independent way, for the stars in common to the two samples. They derived distances calculating the luminosities in a way similar to Eq. (1), but using the bolometric correction at $2.20 \mu\text{m}$, based on a colour index [2.20–3.77] instead. They assumed an absolute magnitude of -5.01 . The mass loss rates are derived from a relation between mass loss and [2.20–3.77] colour, which is based on a previously derived relation between mass loss and $[K - L']$ colour.

Table 3 gives the ratio of the mass loss rates, as well as the distance LeBe2001 would have obtained using the absolute bolometric magnitude derived in this work. With two exceptions, the distances in the present work are significantly larger, by a factor 1.1–3.5, with a median value over all determinations of 1.6. The same trend applies for the mass loss rates which are larger by a factor of about 5 (median value). This is largely due to the fact that the larger distance scale in the present work implies also larger mass loss rates through the square-dependence of mass loss on distance (see Eq. (3)). This suggests a remaining intrinsic systematic uncertainty in the mass loss rate determinations between the present work and LeBe2001 of about a factor of 2. This is within the usu-

ally adopted range of uncertainty in mass loss determinations and can be due to the adopted CO abundance relative to H_2 in our method, or assumptions behind the method in LeBe2001 which is based on modelling the dust emission, and which has its own uncertainties.

The difference in distance scale must be due to the determination of m_{bol} , hence the bolometric correction, which is based on IRAS colours in the present work and basically $[K - L']$ in the case of LeBe2001. As a test, m_{bol} is derived for the best studied (infra red) carbon star, IRC +10 216. We find $m_{\text{bol}} = 0.00$, which leads to a distance of 111 pc for the adopted $M_{\text{bol}} = -5.23$. This distance is in good agreement with the generally accepted distance to this object (Tuthill et al. 2000 [145 pc], Groenewegen et al. 1998a [110–135 pc], Winters et al. 1994 [170 pc]). Based on the mean K and L' photometry in Le Bertre (1992), $m_{\text{bol}} = 0.28$ is derived using the method in LeBe2001. This implies that for IRC +10 216 the method used in LeBe2001 leads to a *longer* distance than the method used in the present work, contrary to the general trend observed in Table 3. Regarding the mass loss rate of IRC +10 216, applying the formalism in LeBe2001 leads to a mass loss of $1.6 \times 10^{-5} M_{\odot} \text{ yr}^{-1}$, in good agreement with the value of $1.5 \times 10^{-5} M_{\odot} \text{ yr}^{-1}$ in the present work. In conclusion, it remains unclear why there are these systematic effects in the two methods of bolometric correction determination. In any case, as the distance dependence of the mass loss rates is explicitly given, our results can be easily scaled to any preferred distance scale.

The most striking result coming out of the present analysis is the dependence of the expansion velocity on galactic longitude. Theoretically, one expects a dependence of the expansion velocity on the gas-to-dust ratio (Ψ), luminosity and mass loss rate (Habing et al. 1994, or, more rigorously derived in Elitzur & Ivezić 2001, who find: $v_e^3 = A\dot{M}(1 + B\dot{M}^{4/3}/L)$, with the dependence on the gas-to-dust ratio contained in the parameters A and B). Neglecting the term between brackets to first order, and since \dot{M} does not depend on galactic longitude (Fig. 4, top panel), one would expect A to show the same kind of dependence on galactic longitude as v_e . As $A \sim \Psi^{-2}$ (Elitzur & Ivezić 2001), one expects the gas-to-dust ratio also to depend on galactic longitude. This is indeed hinted at in Fig. 4 (bottom panel), although formally, as mentioned before, the linear and quadratic terms in the fit are not significant. However, the expansion velocity is a directly measured quantity, while Ψ is a derived quantity, so that any intrinsic effect that is present or expected is smeared out. In conclusion it seems probable that the variation of the expansion velocity with galactic longitude is indeed due to a higher gas-to-dust ratio outside the solar circle than inside.

This appears the first direct confirmation to this effect for carbon stars. Blommaert et al. (1993) found a similar trend by comparing OH/IR stars of similar luminosity in the Galactic centre and outer Galaxy. van Loon et al. (2001) discuss the results of expansion velocity determinations of OH maser sources in the LMC and compare them to determinations of Galactic centre OH maser sources. Their data suggests that the expansion velocity in the LMC sources might be about 20%

Table 3. Comparison of distance (in kpc) and mass loss estimates.

IRAS-name	M_{bol} (this work)	d (this work)	d (LeBe2001)	d (LeBe2001, corrected)	d (this work/LeBe2001)	ratio \dot{M}
02596+6639	-5.02	4.88	2.53	2.54	2.54	4.1
04449+4951	-4.96	2.07	1.94	1.90	1.90	2.9
05426+2040	-4.98	1.25	0.40	0.40	0.40	27.9
11318-7256	-4.96	0.72	0.60	0.58	0.58	6.3
17209-3318	-5.29	3.44	1.72	1.96	1.96	–
18306+3657	-4.96	1.38	0.38	0.37	0.37	64.0
19248+0658	-4.95	2.02	1.37	1.33	1.33	4.3
20084-1425	-4.99	3.45	1.33	1.31	1.31	5.7
21262+7000	-4.71	1.75	0.67	0.51	0.51	19.1
06230-0930	-4.96	2.19	4.46	4.35	4.35	1.9
07098-2012	-5.39	1.66	1.18	1.41	1.41	3.2

lower than for Galactic centre sources of similar OH peak flux, but the data are also consistent with no difference in expansion velocity.

Andrievsky et al. (2002) derive a metallicity gradient of -0.03 dex/kpc in the solar neighbourhood based on classical Cepheids and give references to a large body of previous work (mostly values between 0.0 and -0.1 dex/kpc). If average values of $v_e = 21.1$ km s $^{-1}$ (at a distance of the Galactic centre of 6.5 kpc), and 17.1 km s $^{-1}$ (at 10.5 kpc) are taken, one derives a dependence $v_e \sim Z^\alpha$ with $\alpha = 0.76$, respectively 0.23 , for a metallicity gradient of -0.03 , respectively -0.10 dex/kpc. If one assumes $\Psi \sim Z^{-1}$ then the theoretically expected value of $\alpha = (2/3)$ suggests a metallicity gradient of slightly less than -0.03 dex/kpc.

Acknowledgements. This program was initiated, and part of the observations were obtained, when MG was a research fellow at the Max-Planck Institut für Astrophysik, Garching, Germany. This research has made use of the SIMBAD database, operated at CDS, Strasbourg, France. Thanks to Joris Blommaert for useful discussions and René Oudmaijer for commenting upon an earlier version of the manuscript.

References

- Andrievsky, S. M., Kovtyukh, V. V., Luck, R. E., et al. 2002, *A&A*, 381, 32
- Arndt, T. U., Fleischer, A. J., & Sedlmayr, E. 1997, *A&A*, 327, 614
- Blommaert, J. A. D. L., van der Veen, W. E. C. J., & Habing, H. J. 1993, *A&A*, 267, 39
- Claussen, M. J., Kleinmann, S. G., Joyce, R. R., & Jura, M. 1987, *ApJS*, 65, 385
- Elitzur, M., & Ivezić, Z. 2001, *MNRAS*, 327, 403
- Fleischer, A. J., Gauger, A., & Sedlmayr, E. 1992, *A&A*, 266, 321
- Groenewegen, M. A. T., Baas, F., Blommaert, J. A. D. L., et al. 1999, *A&AS*, 140, 197
- Groenewegen, M. A. T., Baas, F., de Jong, T., & Loup, C. 1996, *A&A*, 306, 241
- Groenewegen, M. A. T., de Jong, T., van der Bliëk, N. S., et al. 1992, *A&A*, 253, 150
- Groenewegen, M. A. T., & de Jong, T. 1998, *A&A*, 337, 797
- Groenewegen, M. A. T., Sevenster, M., Spoon, H. W. W., & Perez, I. 2002, *A&A*, 390, 501 (G2002)
- Groenewegen, M. A. T., van der Veen, W. E. C. J., & Matthews, H. E. 1998a, *A&A*, 339, 489
- Groenewegen, M. A. T., & Whitelock, P. A. 1996, *MNRAS*, 281, 1347
- Groenewegen, M. A. T., Whitelock, P. A., Smith, C. H., & Kerschbaum, F. 1998b, *MNRAS*, 293, 18
- Guglielmo, F., Le Bertre, T., & Epchtein, N. 1998, *A&A*, 334, 609
- Habing, H. J., Tignon, J., & Tielens, X. 1994, *A&A*, 286, 523
- Höfner, S., & Dorfi, E. A. 1997, *A&A*, 319, 648
- Jones, T. J., Bryja, C. O., Gehrz, R. D., et al. 1990, *ApJS*, 74, 785
- Jura, M. 1988, *ApJS*, 66, 33
- Jura, M. 1991, *A&AR*, 2, 227
- Jura, M., & Kleinmann, S. G. 1989, *ApJ*, 341, 359
- Josselin, E., Loup, C., Omont, A., et al. 1998, *A&AS*, 129, 45
- Kastner, J. H., Forveille, T., Zuckerman, B., & Omont, A. 1993, *A&A*, 275, 163
- Kerschbaum, F., & Olofsson, H. 1998, *A&A*, 336, 654
- Kholopov, P. N., Samus, N. N., Frolov, M. S., et al. 1985, *General Catalog of Variable Stars (GCVS)*,
- Knapp, G. R., Young, K., Lee, E., & Jorissen, A. 1998, *ApJS*, 117, 209
- Le Bertre, T. 1992, *A&AS*, 94, 377
- Le Bertre, T., Matsuura, M., Winters, J. M., et al. 2001 *A&A*, 376, 997 (LeBe2001)
- Loup, C., Forveille, T., Omont, A., & Paul, J. F. 1993, *A&AS*, 99, 291
- Loup, C., Groenewegen, M. A. T., Cioni, M.-R., Fouqué, P., & Cohen, M. 2002, in preparation
- Nakashima, J., Jiang, B. W., Deguchi, S., Sadakane, K., & Nakada, Y. 2000, *PASJ*, 52, 275
- Neri, R., Kahane, C., Lucas, R., Bujarrabal, V., & Loup, C. 1998, *A&AS*, 130, 1
- Olivier, E., Whitelock, P. A., & Marang, F. 2001, *MNRAS*, 326, 490
- Olofsson, H. 1993, in *Mass loss on the AGB and beyond*, ed. H. Schwarz (ESO), 330
- Sevenster, M. N., DeJonghe, H., & Habing, H. J. 1995, *A&A*, 299, 689
- Sevenster, M. N., Dejonghe, H., Van Caelenberg, K., & Habing, H. J. 2000, *A&A*, 355, 537
- Schöier, F. L., & Olofsson, H. 2001, *A&A*, 368, 969
- Tuthill, P. G., Monnier, J. D., Damchi, W. C., & Lopez, B. 2000, *ApJ*, 543, 284
- van Loon, J. Th., Zijlstra, A. A., Bujarrabal, V., & Nyman, L.-A., 2001, *A&A*, 368, 950
- Whitelock, P. A., Marang, F., & Feast, M. 2000, *MNRAS*, 319, 728
- Winters, J.-M., Dominik, C., & Sedlmayer, E. 1994, *A&A*, 288, 255